JOURNAL OF Materials CHEMISTRY

Hybrid polydimethylsiloxane–zirconium oxo nanocomposites. Part 1 Characterization of the matrix and the siloxane–zirconium oxo interface

Céline Guermeur,[a] Jacques Lambard,[b] Jean-François Gerard[c] and Clément Sanchez*[a]

[a] *Laboratoire de Chimie de la Matière Condensée, UMR CNRS 7574, Université Pierre et Marie Curie, 4 place Jussieu, 75252 Paris, France*
[b] *Service de Chimie Molèculaire, CEA, CEN Saclay, Gif sur Yvette, France*
[c] *Laboratoire des Matériaux Macromoléculaires, UMR CNRS 5627, INSA de Lyon, 20 Avenue A. Einstein, 69621 Villeurbanne cedex, France*

Received 18th September 1998, Accepted 10th December 1998

Hybrid materials made from polydimethylsiloxane and zirconium oxo species have been synthesized. They exhibit a high degree of homogeneity and dispersion for Zr/Si molar ratios ranging between 0.2 and 0.9. These hybrid materials show good mechanical integrity and transparency. They have been characterized by ^{29}Si, ^{17}O and ^{13}C MAS-NMR as well as FTIR, SAXS and dynamic mechanical analysis (DMA). These polydimethylsiloxane/zirconium oxopolymers are hybrids which consist of amorphous zirconium oxo domains of about one to two nanometers in diameter. The mean corrrelation distance between the zirconium–oxo domains decreases from about 6 to 2 nm when the Zr/Si ratio increases. The siloxane species (chains and loops) have an average chain length that decreases from approximatively 15–20 silicon atoms to 3 silicon atoms with increasing zirconium content. The interface between siloxane and zirconium oxo domains is composed primarily of Zr–O–Si$(CH_3)_2$ bonds and hydrogen bonds, their relative proportion being a function of the zirconium content. The curing of these hybrid materials at 140 °C completes consolidation of the hybrid network, without affecting the overall characteristics of the organic–inorganic interface. Curing at 200 °C induces the loss of small silicic species and the increase of cross-linking points in the siloxane regions. For samples with a high zirconium content (Zr/Si = 0.9) curing at 200 °C also induces an increase in the number of the Zr–O–Si interface bonds.

Introduction

Sol–gel chemistry (metallo-organic precursors, organic solvents, low processing temperatures, mixing at the molecular level) permits the introduction of organic moieties or molecules within an inorganic network. Inorganic and organic components can then be mixed at the nanometric scale in virtually any ratio, leading to hybrid organic–inorganic nanocomposites.[1] For many years metallo-organic precursors, such as metal alkoxides [M$(OR)_n$] have been used *via* hydrolysis–condensation reactions to synthesize oxo-metallic species that act as cross linking reagents for many polymers, including polydimethylsiloxane (PDMS).[2–10] PDMS derived materials are known for their excellent relaxation properties, and only a few hybrid materials containing PDMS moieties experience cracking problems during curing and drying. Moreover, siloxane/metal oxide hybrid materials can successfully incorporate organic dyes or rare-earth elements which retain their optical properties.[11–14] Interestingly, materials containing transition metal oxo species can also modify the refractive index or vary the oxidation state leading to optical, electronic, magnetic or catalytic properties.[11,12]

PDMS based hybrid materials are thus widely studied. Wilkes[9] and Mark[10] simultaneously developed a new kind of composite material made by condensing silanol or alkoxysilyl terminated telechelic polydimethylsiloxane polymers, and tetraethoxysilane. They obtained materials with interesting and modulatable mechanical properties. Transparent hybrids much harder than organic polymers, but less brittle than silica, were thereby obtained.[1c,9,10]

Another approach is to generate *in situ* both the polydimethylsiloxane and the metal oxo species from hydrolysis and condensation of molecular precursors such as diethoxydimethylsilane [$SiMe_2(OEt)_2$] and various metallic alkoxides, M$(OR)_n$ (M = Si, Ti, Zr, Al, VO).[3,14–18] This approach has been widely described in the literature.[3,14–18] It allows true mixing of both components at the nanometric level. The degree of phase dispersion of the metal M in siloxane–metal oxide based matrices depends strongly on the nature of the metal and on the M/Si ratio. Titanium oxide–siloxane and zirconium oxide–siloxane based hybrids generally exhibit a less efficient degree of dispersion than silica based or vanadium oxo based analogs.[3,14–18] The cleavage of $(CH_3)_2$Si–O–M bonds (M = Ti, Zr) upon sol aging as evidenced through ^{17}O NMR,[17b] is probably responsible for the observed tendency. Hybrid materials generated from diethoxydimethylsilane molecular precursors present, as their PDMS-based analogues, siloxane long chains with high mobility together with siloxane moieties in a constraint titania or zirconia environment. This was observed by titanium X-ray absorption, ^{29}Si MAS as well as CP-MAS NMR experiments.[14,19] Phase separation within these siloxane–metal oxide materials was observed but little was known about the size of the different domains, the nature of the siloxane–zirconium oxo interface and the structural modifications occurring on these materials upon thermal curing.

The nature and the extent of the siloxane–zirconium oxo interface play a significant role in controlling the mechanical properties of hybrid materials and their chemical reactivity towards incorporated dyes.[1c,12] Porphyrin dyes carrying different functional groups have been embedded and grafted in these siloxane–zirconium oxo hybrid networks. A forthcoming paper will describe the nature of the interactions undergone by different porphyrins as evidenced by their absorption–emission properties. Room temperature processed sol–gel hybrid matrices can evolve with time, thereby complicating our understanding of structure–property relationships.[12,20–22] Thermal curing at temperatures below 250 °C, to avoid dye degradation, can be used to stabilize the hybrid matrix. However, little

is known about the influence of curing at relatively low temperature on hybrid materials.

In order to elucidate the structure–property relations this article describes the synthesis and characterization by ^{29}Si, ^{17}O, ^{13}C MAS NMR, FTIR and SAXS of hybrid siloxane–zirconium oxo matrices, before and after thermal curing. The evolution of their structure and mechanical properties is also discussed. Special attention will be devoted to the characterization of the interface between the organic (siloxane species) and inorganic (zirconium oxo species) components.

Experimental

Sample preparation

The hybrid matrices were prepared following a procedure previously described.[14] 10 g of dimethyldiethoxysilane [$(CH_3)_2Si(OC_2H_5)_2$; Fluka], 3.1 g of absolute ethanol and 1.2 ml of acidified water (0.1 M hydrochloric acid solution) were mixed and magnetically stirred. After five minutes, zirconium propoxide [$Zr(OPr^n)_4$; Fluka] was added to the solutions in order to produce Zr/Si molar ratios ranging from 0.2 to 0.7. One to two milliliters of these sols were poured into vessels and allowed to dry slowly. After three weeks drying in air at room temperature bulk samples were obtained. Four different compositions were prepared and the bulks were labeled B1 to B4, the zirconium content increasing with the sample number. 5.5 g, 9.5 g, 14.7 g and 22.1 g of 70 wt% $Zr(OPr^n)_4$ in propanol were used for the syntheses of samples B1 to B4 respectively. Densities, measured by weighing the samples in air and in water, were 1.2 g cm^{-3} and 1.7 g cm^{-3} for samples B1 and B4 respectively. The initial Zr/Si molar ratios were 0.17 (B1), 0.30 (B2), 0.47 (B3) and 0.70 (B4).

Chemical and spectroscopic characterizations (see Results and discussion section) show that all the hybrid xerogels described in this article are highly condensed. Fully condensed materials should have the general composition $(SiMe_2O)_x$-$(ZrO_2)_{(1-x)}$. The stoichiometric amount of water needed for the formation of this materials is 0.5 mole for each alkoxy group. In the syntheses of B1 to B4, the amount of water added to the sol is not sufficient to fully hydrolyze and condense all present species. Air moisture provides the necessary water to complete the condensation reactions. The amount of water provided by air moisture increases as x decreases.

B1 can be shaped easily, is transparent and mechanically strong. The characterization of B1 type matrices, which are used as a hosts for organic dyes,[13,20] will be more extensively presented than the other samples. As for many other hybrids thermal curing can be used to stabilize the matrix. A study of the influence of the thermal curing on the structure and properties of B1 has been performed. More precisely, work has been focused on curing at temperatures lower than 250 °C which do not lead to degradation of organic dyes such as phthalocyanines or porphyrins. B1 was cured at 140 and 200 °C under nitrogen for 15 h. The resulting samples are respectively labeled B1-140 and B1-200. Some interesting results obtained with B4 cured at 200 °C under nitrogen for 15 h, labelled B4-200, will also be presented.

The zirconium to silicon molar ratio in the dried bulk hybrid samples obtained from chemical analysis was consistently higher than the initial composition of the sols. For example, the Zr/Si ratio increases from 0.17 to 0.23 and from 0.7 to 0.91 for B1 and B4, respectively. Moreover, upon thermal curing this ratio increases to 0.24 and 0.30 for B1-140 and B1-200, respectively. This systematic increase of the Zr/Si ratio can be assigned to silicon loss during the drying step through evaporation of volatile cyclic siloxane species which are present in the sol.

B1 bulk samples can be easily swelled in nonpolar solvents such as benzene or cyclohexane, leading to soluble and insoluble fractions. This behavior is well known in silicone chemistry[23] and is usually assigned to the partial solubilization of noncrosslinked oligomeric linear or/and cyclic siloxane species.

B1 bulk samples can be fully dissolved in acetylacetone. The resulting sol was also characterized in order to improve our knowledge of this hybrid system.

Infra-red spectroscopy

The Fourier transform infra-red (FTIR) spectra of the samples were recorded on a Nicolet Magna-IR 550 spectrometer in the 4000–400 cm^{-1} frequency range with a resolution of 2 cm^{-1}. The xerogel samples were pelleted with dried KBr. Similar FTIR spectra were also recorded directly on thin bulk samples using the ATR technique.

NMR experiments

All nuclear magnetic resonance (NMR) spectra were recorded on a MSL 300 Bruker spectrometer. For the ^1H magic angle spinning (MAS) NMR spectra, the experimental conditions were: 1 ms pulse, recycle delay 5 s, spinning frequency 15 kHz. ^{29}Si MAS NMR data were recorded under the following experimental conditions: 2 ms pulse, recycle delay 10 s, spinning frequency 4 kHz. The delay of 10 s between two consecutive pulses was sufficient to obtain quantitative results. As for the ^{29}Si cross-polarization (CP) MAS technique, the experimental conditions were: recycle delay 10 s, duration of the ^1H 90° pulse 6 ms, contact time 3 ms, spinning frequency 4 kHz. ^1H and ^{29}Si isotropic chemical shifts are referenced to TMS. The ^1H and ^{29}Si NMR spectra were simulated and the signal intensities determined using the WIN-FIT program.[24]

The natural abundance of oxygen-17 is very low (0.037%), making difficult the recording of spectra on naturally enriched samples. All samples characterized using ^{17}O NMR were synthesized using 10% or 20% oxygen-17 enriched water for the hydrolysis of the dimethyldiethoxysilane precursor. The addition of enriched water to metal alkoxide precursors results in a selective enrichment of the metal–oxo bridges of the oxopolymers. The enrichment process can be schematically described as follows:

$$\ldots M\text{–}OR + H_2O^* \rightarrow \ldots M\text{–}O^*H + ROH \quad \text{hydrolysis}$$

$$\ldots M\text{–}O^*H + M\text{–}OX \rightarrow \ldots M\text{–}O^*\text{–}M\ldots + XOH \quad \text{condensation}$$

R is an alkyl chain and X an alkyl chain or a proton.

Compared to selective enrichment of metal–oxo bridges, and the terminal and bridging hydroxy groups, the unenriched alkoxy groups can be considered as ^{17}O NMR silent.

The experimental conditions for recording ^{17}O MAS NMR conditions were: 2.9 μs pulse, recycle delay 0.2 s, spinning frequency 5 kHz. ^{17}O isotropic chemical shifts are referenced to water.

Small angle X-ray scattering (SAXS)

The structure of the hybrid materials was investigated by small angle X-ray scattering. SAXS experiments were performed on a Bonse–Hart diffractometer developed at the CEA (Saclay, France). Complete experimental details for this set-up were provided in a previous report.[25] Two wavelengths were used: 1.54 Å (copper Kα line) and 0.7 Å (molybdenum Kα line). Air scattering was subtracted from the SAXS data of the samples.

Mechanical properties and thermal analysis

Differential scanning calorimetry (DSC) measurements were performed on hybrid xerogels from 77 K to room temperature using a Perkin-Elmer DSC7 apparatus. The heating rate was 20 °C min^{-1}. Dynamical mechanical analysis (DMA) was performed using a specimen size of 20 mm × 5 mm × 2 mm with a

TA Instruments DMA 29-80 apparatus operating at 1 Hz from -150 to $+150\,^{\circ}C$.

Thermogravimetric analysis (TGA) was carried out using a Netzsch STA 409 apparatus with a heating rate of $10\,^{\circ}C\,min^{-1}$ under an oxygen flow.

Results and discussion

Experimental results pertaining to the characterization of the siloxane and inorganic components and their interface are presented in the first part of this section. Subsquently the thermal behavior and mechanical properties of the hybrid materials are given. In the second part of this section the main results are summarized and discussed.

FTIR spectroscopy

Infrared absorption experiments were carried out as a function of composition and curing temperature. FTIR spectra of B1 and B4 hybrids are presented in Fig. 1(a) and (b) respectively. B2 and B3 FTIR spectra are not reported because they do not present major differences with respect to those reported for B1 and B4.

FTIR spectra of B1 and B4 exhibit absorption bands whose maxima are located at 2964, 2908, 1262 and $800\,cm^{-1}$. These bands are characteristic of the siloxane component, and are assigned to symmetric and antisymmetric CH stretching vibrations, to CH_3 bending mode and to CH_3 bending mode coupled to SiC_2 stretching vibrations, respectively. The intensities of two other absorption bands increase with the zirconium content: the first one which is broad and is located around $3410\,cm^{-1}$ is due to OH stretching vibrations. These hydroxyl groups can belong to water molecules or to silanol goups linked to water by hydrogen bonds. The second band is located at $1630\,cm^{-1}$ and is due to the deformation mode of molecular H_2O. These results show that retention of water in the hybrid material is more efficient as the zirconium content increases, due to the contribution of hydrophilic regions of zirconium oxopolymers.

A weak absorption band located at $3774\,cm^{-1}$ appears for all compositions despite the fact that the water content is increasing. It is assigned to the stretching mode of free silanol groups (no hydrogen bonding) and reveals the presence of strong hydrophobic regions separated from the hydrophilic ones.

In the absorption domain ranging between 900 and $1200\,cm^{-1}$ four main peaks are observed at 940, 980, 1021 and $1098\,cm^{-1}$. The band at $940\,cm^{-1}$ is assigned to the Si–OH stretching vibration, generally observed between 930 and $980\,cm^{-1}$ in many silica based sols or gels.[26] The IR band located at $980\,cm^{-1}$ appears as a shoulder in the FTIR spectrum of B2 and increases in intensity with the zirconium content. This absorption band is also visible for the lowest zirconium content (sample B1) after Fourier self deconvolution

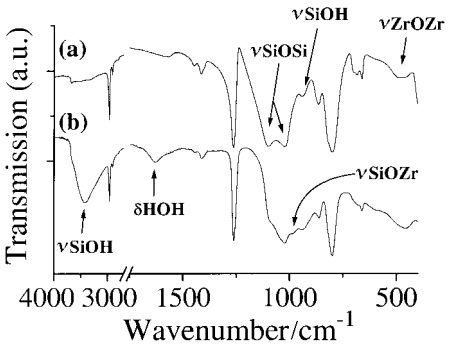

Fig. 1 FTIR spectra of (a) B1 and (b) B4 samples. The transmission is given in arbitrary units but both spectra are at the same scale.

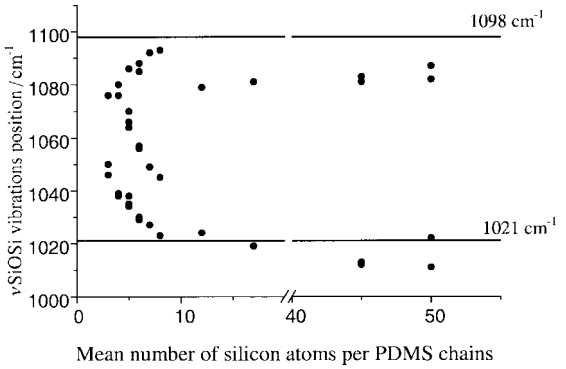

Fig. 2 Maxima of the νSiOSi vibration bands for various commercial PDMS (full lines represent the position of maxima recorded for B hybrids).

of the IR spectra. Stretching vibrations characteristic of the Si–OM bonds (M being a metal atom heavier than silicon), have been reported at $945\,cm^{-1}$ for tin[27] and at $950\,cm^{-1}$ for titanium.[28] Absorption bands located at 970 or $980\,cm^{-1}$ observed in the IR spectra of xerogels obtained from hydrolysis and condensation of silicon and zirconium alkoxides have been assigned to Si–OZr stretching vibrations.[29] This assignment is still a matter of debate.[30] However for all the present hybrid materials a good correlation between the intensity of the absorption band at $980\,cm^{-1}$ and the zirconium content was observed. This correlation allows the assignment of this band to Si–OZr stretching vibrations.

The broad signal with two maxima centered around 1021 and $1098\,cm^{-1}$ is assigned to Si–O–Si stretching vibrations. These two maxima are often observed in polydimethylsiloxane oligomers, polymers and networks. Mauritz *et al.*[31] in their IR study on perfluorosulfonate–dimethyldiethoxysilane based hybrids proposed to assign the low energy band ($1030\,cm^{-1}$) and the high energy band ($1080\,cm^{-1}$) to ν(Si–O–Si) vibrations, characteristic of cyclic and linear difunctional species, respectively. A plot of the published position of these two maxima *versus* the mean number of silicon atoms for several PDMS species is presented in Fig. 2. The position of the low energy band for the present materials ($1020\,cm^{-1}$) is in agreement with published infra-red data on polydimethylsiloxane chains having a mean number of silicon atoms higher than 10.[32,33] Considering Mauritz's assignments,[31] the $1090\,cm^{-1}$ IR band which has an energy and a relative intensity higher than those reported for all linear polydimethylsiloxanes could be assigned to the contribution of cyclic species (probably in the form of large loops). However, the position of this band is also influenced by the proximity of Zr atoms.

The broad IR absorption band located around $460\,cm^{-1}$ is characteristic of the Zr–O–Zr stretching vibration and shows the formation of a zirconium oxo network. This is consistent with the fact that hydrolysis of tetravalent metal alkoxides (zirconium or titanium alkoxides) in many hybrids leads to the formation of metal oxo clusters and amorphous oxopolymers.[19,33]

The FTIR spectra of cured B1-140 and B1-200 show almost no difference compared to B1. In the case of B4-200, two main trends can be seen. Fistly, there is a decrease in the intensity of the νOH band around $3400\,cm^{-1}$ and, secondly a clear modification of the shape of the 900–$1200\,cm^{-1}$ region. Although the structure of this absorption domain is complex, the observed change can be tentatively assigned to an increase in the contribution of the absorption band corresponding to Si–OZr vibrations band at $980\,cm^{-1}$.

^{1}H MAS NMR study

The ^{1}H MAS NMR spectrum of B1 (Fig. 3) presents one very sharp resonance located at 0.2 ppm and no rotational bands.

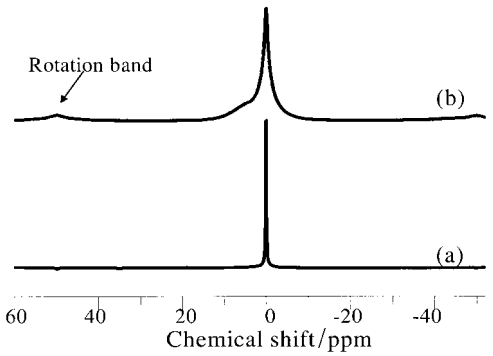

Fig. 3 ^{1}H MAS NMR spectra of (a) B1 and (b) B4.

This resonance can be assigned to methyl protons of dimethylsiloxane moieties (PDMS species). The B4 MAS NMR spectrum exhibits two broader resonances with rotational bands [Fig. 3(b)]. The broadening of the signal with increasing zirconium content can be associated with a decrease in the PDMS chain mobility. Deconvolution of the MAS NMR spectra indicates that the two maxima of the resonances are located at 0.2 ppm and 4 ppm. Their relative intensities are 75 and 25% of the total NMR signal, respectively. The weaker resonance can be assigned to hydroxy protons in water, silanol groups or residual alcohol.

The ^{1}H MAS NMR spectra for B1-140 and B1-200 are very similar to B1. The main difference observed is a slight broadening of the resonance at 0.2 ppm assigned to methyl protons of PDMS.

^{29}Si MAS NMR experiments

Fig. 4 shows the ^{29}Si MAS NMR spectra of B1, B3 and B4. The sharp resonance at -22.3 ppm is characteristic of Si atoms in a linear dimethylsiloxane polymer backbone.[34] In agreement with ^{1}H NMR experiments, the narrow linewidth of the ^{29}Si NMR signals reflects the high mobility of these species. Although these samples are solids, the mobility of the methyl groups is sufficient to average the dipolar Si–H interaction. For B1 the -22.3 ppm resonance is the only one observed, whereas B3 and B4 signals are dissymmetric suggesting the presence of other broad resonances with maxima located around -20 ppm. These two types of resonances have already been observed for polysiloxane/transition metal oxide hybrids.[3,14–17] The broad component has been assigned mainly to $Me_2Si(OSi\equiv)_2$ units in a constrained environment near the transition metal oxo polymers. For B3 the broad part of the NMR signal spreads down to the chemical shift range where

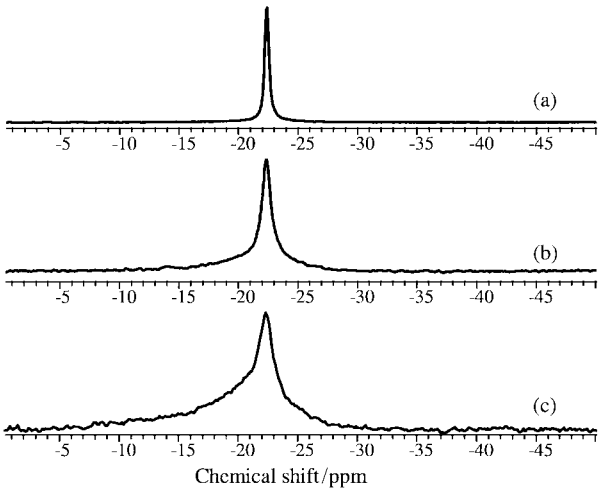

Fig. 4 ^{29}Si MAS NMR spectra of (a) B1, (b) B3 and (c) B4.

Table 1 Fitted relative intensities between the sharp and broad ^{29}Si NMR resonances

Sample	Broad/sharp resonances area ratio
B1	0
B3	1.1
B4	4.5

D_1 units are expected. These D_1 species are Me_2Si(OSi)OX species, where X is H or an alkyl group and their chemical shift is in the -10 to -16 ppm region (dimethylsiloxane species). This phenomenon is even more distinct for B4. The large linewidth of this broad component is mostly due to a decrease in the siloxane unit mobility possibly linked to more rigid zirconium oxo metallic clusters or located in their proximity.

The three spectra can be fitted by taking into account three components: one sharp component located at -22.3 ppm and two broad resonances at -21.6 and -17.8 ppm. The linewidth of the sharp resonance increases with zirconium content suggesting that the siloxane regions are in a more rigid environment. Schematically the sharp resonance at -22.3 ppm corresponds to silicon atoms (D_2 units in a siloxane sequence) located in the middle of PDMS chains or in loops, whereas the broad resonances could be due to silicon atoms at the ends or close to the ends of these siloxane sequences. The fitted relative intensities between the sharp and broad resonances are reported in Table 1. The ratio between Si atoms associated with the broad resonances and those corresponding to the sharp one gives an estimate of the mean length of the PDMS polymers or oligomers.

For B1 materials, practically no broad signal can be detected, indicating that silicon atoms located at the ends of the PDMS chains represent less than 10% of the total number of silicon atoms. Two explanations for this observation can be proposed: (i) B1 is made from PDMS chains containing at least about 20 Si atoms, but this number could be lower if the presence of loops (D_2 units without D_1 endings) is taken into account; (ii) B1 contains probably both an important proportion of PDMS loops and PDMS chains containing less than 20 Si atoms. This explanation is in agreement with the observed swelling and dissolution properties. Table 1 shows that PDMS segments are much shorter for B3 and B4 materials which contain on average four Si atoms and less than three Si atoms, respectively.

Thermal treatment at 140 °C does not induce major changes in the ^{29}Si NMR spectra of B1. For B1-200 materials the sharp signal due to $Me_2Si(OSi\equiv)_2$ D_2 units remains unchanged but weak resonances representing about 15% of the total intensity appear at -89.3, -66 and -19.6 ppm. They can be assigned to SiO_4 (Q) units, $MeSiO_3$ (T) units and D_2 units linked to these T or Q species respectively.[35] Curing at 200 °C induces reorganisation of the Si–C bonds. Q and T units induced by thermal treatment will act as crosslinking agents and thus increase the rigidity of the hybrid network (*vide infra*: DMA experiments).

^{29}Si CP-MAS NMR

Mobility can average the dipolar coupling between the Si nuclei and the protons of the methyl groups thereby reducing the cross polarization efficiency. As a result, the intensity of NMR signals corresponding to less mobile silicon species is amplified when the ^{29}Si NMR spectra are recorded using a CP-MAS sequence. Indeed, a broad component is clearly visible on the ^{29}Si CP-MAS NMR spectrum of B1 (Fig. 5). This observation confirms that silicon atoms located at the end of the chains are less mobile than those located inside polysiloxane sequences. This behavior is different from that described in models dealing with the mobility of linear poly-

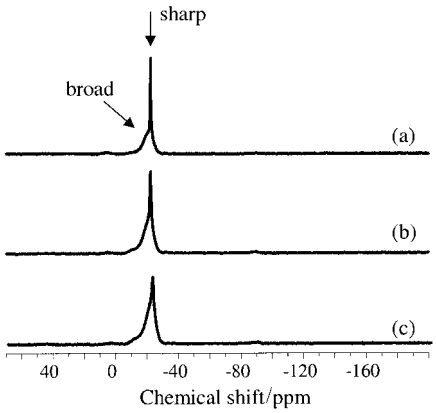

Fig. 5 ^{29}Si CP MAS NMR of (a) B1, (b) B3 and (c) B4.

mers, where the motion of chain ends is usually more important.[36] The broad signals observed in ^{29}Si NMR spectra of these hybrid materials are due to silicon atoms hindered in their motion. The causes of this decrease in mobility are probably the formation of Si–O–Zr bonds between polysiloxane components and zirconium oxo polymer domains, and the formation of hydrogen bonds between residual SiOH moieties and hydrophilic zirconium oxopolymer domains.

^{29}Si NMR experiments on dissolved samples

Dissolution experiments were performed on bulk samples in order to get more information about the different components constituting the B hybrids. About 5 g of xerogel B1 were added without preliminary grinding to 4 ml of acetylacetone while stirring. A diphasic system composed of an oil floating on a tranparent liquid surface is thus obtained. Under the same conditions, the dissolution of B4 leads to the formation of a transparent sol. Bar shaped crystals are formed after a few days in the sols obtained by dissolution of B1 and B4. As confirmed by IR spectroscopy, these crystals correspond to zirconium tetrakis(acetylacetonate), $Zr(Acac)_4$.[37] This suggests that the dissolution phenomenon is probably driven by the intimate association between a swelling process of the siloxane moieties and a redissolution process of the zirconium oxo clusters through complexation reactions involving acetylacetonato ligands.

The addition of 3 ml tetrahydrofuran to the diphasic B1 sol leads to a homogeneous transparent sol for which the ^{29}Si NMR spectrum is presented in Fig. 6(c). For comparison, the ^{29}Si NMR spectra of the sol initially used to prepare B1 and the same sol after addition of acetylacetone are presented in Fig. 6(a) and (b), respectively. The spectrum of dissolved B1

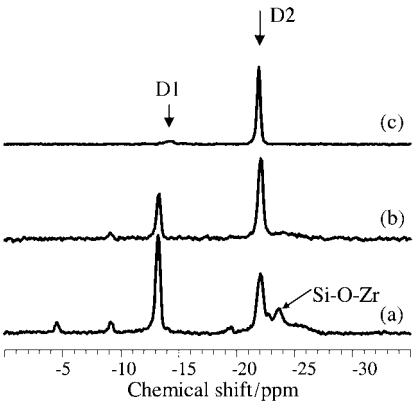

Fig. 6 ^{29}Si NMR spectra of (a) the B1 sol, (b) the B1 sol after addition of acetylacetone and (c) the B1 xerogel dissolved in acetylacetone and tetrahydrofuran.

shows only two resonances located at -14.2 and -21.8 ppm which can be assigned to D_2 units and D_1–OH or D_1–OR units (OR = OEt, Acac), respectively. The area ratio between D_2 and D_1 species is about 6:1. From this value and assuming that the sol is only composed of hydroxy or OR terminated PDMS chains, a mean chain length of about 15 silicon atoms can be calculated.

The appearance of an oily phase in the case of B1 redissolution confirms the presence of long PDMS species. The fact that this oily phase is not observed in the dissolution experiment performed with B4 corroborates the view that siloxane species are much shorter in the B4 hybrid than in B1.

The addition of complexing β-diketone provokes the disappearance of the ^{29}Si NMR resonances located at -23 and -27 ppm, assigned to Si–O–Zr bonds[15,17] (see Fig. 6(a) and (b)). This observation indicates that the dissolution process should find its origin in the cleavage of the Zr–O–Si interface. Such complexation driven redissolution processes have already been observed for polyAAEM–zirconium-oxo hybrids (AAEM = acetoacetoxyethyl methacrylate).[38]

^{17}O MAS NMR spectroscopy

This technique is particularly useful for studying Si–O–M bonds,[17,39] and was used to characterize these polysiloxane/metal oxide hybrids. Fig. 7(a) and (b) show the ^{17}O MAS NMR spectra of B1 and B4, respectively. The assignments of the different ^{17}O NMR resonances are presented in Table 2.

The resonances located at 410 and 380 ppm represent ^{17}O–Zr_3 species while the one at 290 ppm can be assigned to ^{17}O–Zr_4 species.[40,41] These resonances due to $^{17}OZr_x$ species have the same shape and relative ratio as those reported for zirconium oxo amorphous xerogels synthesized through the hydrolysis of zirconium alkoxide precursors.[42] The local structure of the zirconium oxo inorganic domains of the hybrid materials presented in this work is then probably not modified by the PDMS moities. The sharper ^{17}O NMR resonance at 340 ppm may be due to some residual molecular $^{17}OZr_4$ species: such sharp resonances are usually observed when zirconium *n*-propoxide based sols are hydrolyzed with low hydrolysis ratios ($H_2O/Zr < 1$). This condition is known to

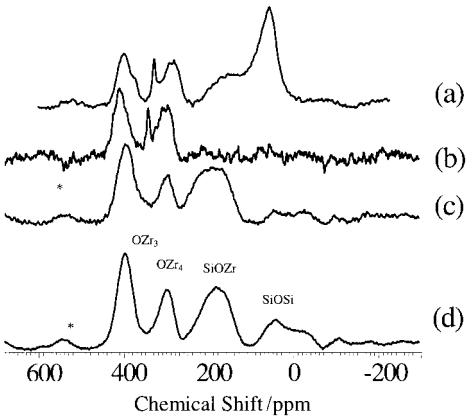

Fig. 7 ^{17}O MAS NMR spectra of (a) B1, (b) B4, (c) B4-200 and (d) B4 dried in an $H_2{}^{17}O$ enriched atmosphere and cured at 200 °C.

Table 2 Assignments of the different ^{17}O NMR resonances

Chemical shift/ppm	Assignment
410	OZr_3
380	OZr_3
340 (sharp)	OZr_3 or OZr_4 (molecular species)
290	OZr_4
170	OZrSi
40–70	OSi_2

favor the formation to transition metal oxo-alkoxo clusters.[33b,43,44] The main resonance located at 70 ppm is due to bridging $^{17}OSi_2$.[45]

The broad signal located around 170 ppm can be assigned to Si–^{17}O–Zr bonds.[17b,39] This directly reveals the presence of a covalent interface between the zirconium oxo and siloxane domains.

Thermal treatments of B1 at 140 and 200 °C have little influence on the B1 ^{17}O NMR spectrum. The only observed modification is the disappearance of the sharp resonance at 340 ppm. This modification can be associated with cluster collapse during thermal curing. For B4, the thermal curing leads also to the disappearance of the sharp 340 ppm resonance. The most important modification of the ^{17}O NMR spectrum is the growth of a broad resonance around 170 ppm assigned to Si–^{17}O–Zr bonds. This large increase cannot be provided by oxygen-17 atoms coming from residual enriched water molecules, residual enriched silanol groups or even siloxy groups because the ^{17}O NMR resonances corresponding to these species are very weak and undetected for uncured samples. As a result, the oxygen-17 atoms involved in the increase of this resonance originate from some $^{17}OZr_x$ species which have been redistributed upon curing.

It is interesting to point out that the intensities of the $^{17}OSi_2$ resonances recorded on ^{17}O enriched B4 (cured and uncured) are always much weaker than those expected in view of the xerogel chemical compositions (Fig. 7). Moreover, as evidenced through ^{17}O NMR and ^{29}Si NMR, almost all the water added for hydrolysis is consumed to form siloxane oligomeric species[17] as the zirconium propoxide precursor is added to the sol. Thus, in dried bulk hybrids the Si–O–Si backbone is mainly formed with NMR silent oxygen-16 while initially the oligomeric siloxane species present in the sol were ^{17}O enriched.[17]

In order to shed more light on this phenomenon the following experiment was carried out: the B4 sol was not dried in air, but in a closed glass vessel flushed with argon, but containing a cupel filled with oxygen-17 enriched water. Thus, in this experiment the additionnal water needed for the synthesis of the bulk hybrid did not come from air moisture but from oxygen-17 enriched water vapor. Gelation and drying in these conditions lead to hybrid bulk samples which were heated up to 200 °C under argon. The ^{17}O NMR MAS spectrum of this sample is presented in Fig. 7(d). Clearly, the resonance assigned to $^{17}OSi_2$ is visible around 45 ppm.

These ^{17}O NMR experiments show that during drying and gelation oxygen atoms are transferred from siloxane species toward zirconium oxopolymer domains. This phenomenon explains the low intensities of the $^{17}OSi_2$ NMR resonances recorded for ^{17}O enriched hybrid samples prepared under the standard air dried conditions. This emphasizes the strong reorganizations that can occur in sols during drying. These reorganizations are the result of numerous solvolysis and condensation reactions probably templated and catalyzed by the zirconium metallic centers which are well known Lewis acid sites.

Small angle X-ray scattering

The most appropriate technique to study the size of small heterogeneities (up to a few Å) in materials is small angle X-ray scattering (SAXS). SAXS data recorded for B1 to B4 are plotted as the scattered intensity *versus* the scattering vector $q(Å^{-1})$ ($q=[(4\pi/\lambda)\sin\theta/2]$). Scattering profiles show a broad maximum (Fig. 8) which is characteristic of correlation between regions of the same electronic densities in a medium of different density. The positions of these SAXS maxima give an estimation of the characteristic distance between these domains. Because the hybrid samples are nonporous, these correlated regions have been assigned to dense zirconium

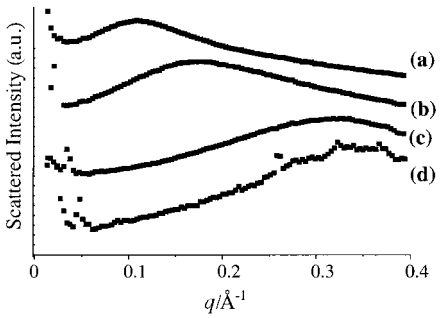

Fig. 8 SAXS diffusion profile ($\lambda=1.54$ Å) of (a) B1, (b) B2, (c) B3 and (d) B4 xerogels.

oxopolymer domains embedded into a low density siloxane matrix. Similar scattering profiles have been reported in SAXS studies of hybrid materials made from PDMS polymers crosslinked with silica or titania based nanoparticles.[46–48] The distance between these zirconium oxo inorganic domains, evaluated from the q values of the scattering maxima, are 5.7 nm, 3.5 nm, 2.2 nm, and 1.7 nm for B1, B2, B3, and B4 respectively. As the zirconium content increases, the zirconium oxopolymer correlation distance decreases down to 17 Å for B4. This result is in agreement with the fact that the volume fraction of zirconium oxopolymers increases with zirconium content. The SAXS profile of the B1-200 hybrid does not show important modifications compared to B1. A broad scattering peak whose maximum corresponds to a correlation distance ζ of about 7 nm is clearly observed.

The approach developed by Beaucage *et al.* has been used[49] to evaluate the mean radius of the oxopolymer domains. It consists of fitting the scattering curves with the following function:

$$I(q)\approx\left\{G\exp\left(\frac{-q^2R_g{}^2}{3}\right)+B\left[\frac{\left(\mathrm{erf}\left(\frac{qR_g}{\sqrt{6}}\right)\right]^p}{q}\right]\right\}\times\frac{1}{1+k\theta}$$

$$\text{with } \theta=3\frac{\sin(q\varsigma)-q\varsigma\cos(q\varsigma)}{(q\varsigma)^3}$$

where: B and G are prefactors; R_g is the gyration radius of the oxopolymer domains; p is the exponent that describes the shape of the curve decreasing at high q values; k is the factor that describes the correlation degree between zirconium oxo domains, and ζ is the correlation radius that can be equated to the interdomains distance $2\pi/q_m$, q_m being the position in q space of the maximum in the scattering curve.

In the case of B4, the maximum of the scattered intensity is located at slightly high wavevectors (short distances). When using a 1.54 Å wavelength, at low q values, a part of the decreasing scattering curve is missing. SAXS experiments have therefore also been registered with 0.7 Å wavelength X-rays for the samples [Fig. 9(b)]. This allowed a better fit of the scattering profiles. A good agreement between fitted and experimental data was obtained, as shown in Fig. 9. The parameter values obtained by fitting the SAXS curves are reported in Table 3. According to these fits, the mean radius of the zirconium oxo domains is in the range of one nanometer. The size of these domains seems to be uninfluenced by the zirconium content. The k factor which describes the correlation degree between zirconium oxo domains decreases from B1 to B4. This evolution reveals a spatial definition of the zirconium oxo domains which increases with zirconium content.

TGA measurements

Thermal analysis data recorded for B1 to B4 are presented in Table 4. Three main weight losses occur in the 20–200, 200–350

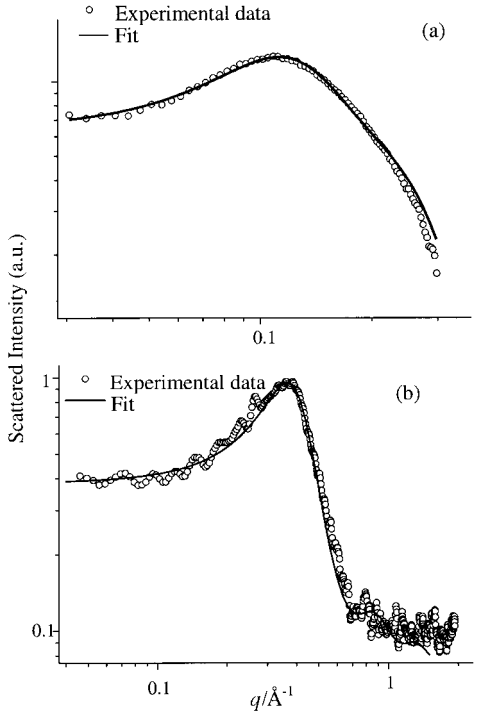

Fig. 9 SAXS scattered intensities (experimental and fitted) for (a) B1 ($\lambda = 1.54$ Å) and (b) B4 ($\lambda = 0.7$ Å) xerogels.

Table 3 Fitted parameters (k, p, B/G, R_g) obtained from SAXS data. R_g is the mean radius of the zirconium oxo domains as measured by SAXS

Sample	k	$\zeta \pm 0.3$/nm	p	B/G	$R_g \pm 0.3$/nm (SAXS results)
B1	1.3	4.5	0.5	0.006	0.8
B4	4.5	1.4	0.5	0.048	0.6

and 350–1000 °C temperature ranges. Between 20 and 200 °C the weight loss is small (4% for B4 and 2% for B1). It corresponds essentially to the departure of alcohol for uncured samples and water for cured ones.

After curing at 200 °C, chemical analysis shows an increase Zr/Si molar ratio from 0.23 for B1 up to 0.30 for B1-200. This rise corresponds to a 15% weight loss, assuming that $(SiMe_2O)_x$ species are lost. Indeed, in this range of temperature, silicon losses are mainly due to the departure of trimeric and tetrameric species [$(SiMe_2O)_3$ and $(SiMe_2O_4)_4$] as verified through mass spectrometer coupled TGA measurements. The departure of similar species, but at temperatures higher than 400 °C, was also observed during the calcination of PDMS/silica hybrid materials.[50] Thermal treatment of the hybrid B samples at temperatures higher than 350 °C leads to a loss corresponding mainly to the departure of $H_xSiMe_{(4-x)}$ and methane.

Curing at 140 °C (B1-140) gives results consistent with the chemical analysis: the Zr/Si ratio is the same for aged B1 and B1-140. The B1-200 exhibits smaller thermal losses than B1 and B1-140. Moreover, the hybrid B1-200 exhibits, in the temperature range 200–350 °C, a 6% weightloss considerably smaller than that recorded for B1 (17%) or B1-140 (16%). These results are consistent with the fact that upon curing at 200 °C many silicic oligomeric species have already been released and evaporated.

Table 4 Thermal analysis data recorded for B1 to B4 samples

$\Delta m/m$ (%)	20–200 °C	200–350 °C	350–850 °C	Total
B4	4	11	8	24
B1	2	17	15	34
B1-140	1	15	16	32
B1-250	1	6	14	21

Mechanical properties

The DSC curves recorded for B1 hybrids exhibit one main thermal feature: a well resolved glass transition at −117, −117 and −114 °C for B1, B1-140 and B1-200, respectively. This observation corroborates the description of B1 hybrids as nanocomposites composed of long PDMS moieties crosslinked by inorganic zirconium oxo domains. The latter do not participate in the glass–rubber transition.

Typical results of dynamical mechanical testing of these PDMS based hybrids are shown in Fig. 10. The storage modulus exhibits a plateau of 2.5×10^9 Pa below −100 °C, which is typical for glassy polymers. As the temperature rises, these hydrid materials exhibit two transitions associated to the observed decrease of modulus. The transitions were determined from the maximun of the loss factor tan δ (Fig. 10). The first transition located around −110 °C is assigned to the backbone motion of the PDMS chains associated with the glass transition, and is located at −117 °C (tan $\delta = 0.26$) for a freshly prepared B1 sample. For B1 cured at 140 and 200 °C the glass transition temperature measured by DMA decreases to −110 °C (tan $\delta = 0.26$) and −103 °C (tan $\delta = 0.16$), respectively. These T_g values are close to those measured by DSC. However DMA experiments seem to reveal more clearly the differences between the hybrid samples. The T_g is estimated to be −123 °C for PDMS of infinite molecular mass[51] and experimental values of T_g recorded on pure PDMS are generally about −120 °C. Hybrid materials made with siloxane species crosslinked by inorganic nanodomains show a noticeable shift of the glass transition temperature to higher temperatures,[9,10,52] especially after thermal curing. In most polymers, crosslinking induces severe constraints on the mobility of the chains, making it more difficult for the chains to participate in the cooperative chain movements associated with the

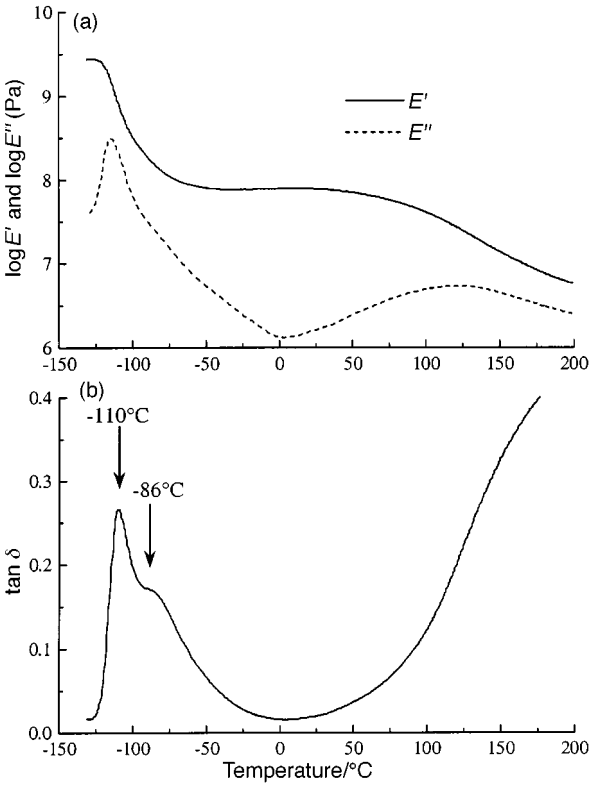

Fig. 10 Dynamic mechanical spectra of B1 hybrid sample *vs.* temperature: (a) evolution of storage and elastic modulus (b) evolution of the loss tangent δ.

glass–rubber transition. Consequently, as observed for the hybrid materials reported in this work, the glass transition can be achieved only at temperatures greater than that for uncrosslinked polymer.

A second broader transition at about $-85\,^{\circ}C$ was also observed by DMA. This kind of broad variation of the loss factor has been previously observed in charged PDMS, containing between 30 and 50 mol% of $Si(OR)_4$ or $Ti(OR)_4$.[9] In some cases, the broad tan δ variation can spread over -110 and $+50\,^{\circ}C$, exhibiting two main maxima, at low temperature and at relatively higher temperatures.[9] These observations result from a continuum of species ranging from PDMS rich phases with low transition temperatures and generally complex crosslinking interfaces, to better dispersed PDMS oligomers (higher transition temperatures) in the midst of network regions resulting from the hydrolysis and condensation of $Si(OR)_4$ or $Ti(OR)_4$. This second transition assigned to more constrained siloxane domains depends slightly on the curing temperature. The maxima are located at $-86\,^{\circ}C$ ($\tan\delta=0.17$) for B1 and B1-140 and at $-84\,^{\circ}C$ ($\tan\delta=0.14$) for B1-200.

After this second broad transition, the modulus reaches a second plateau which expands over $150\,^{\circ}C$. The storage modulus measured at room temperature at the rubbery plateau is about 10 MPa for freshly prepared B1, increasing to about 60–70 MPa for B1 samples aged at $60\,^{\circ}C$ or cured at $140\,^{\circ}C$, and finally reaching a maximum at 100–115 MPa for B1 hybrids cured at $200\,^{\circ}C$. These values are in agreement with those reported for stiff PDMS elastomers.[9,10]

The increase in Young's modulus is associated with more highly crosslinked materials. For B1-200 materials, the increased crosslink density is associated with the formation of T and Q silicon units as revealed by ^{29}Si NMR experiments.

The main results concerning structural characterization of these hybrid materials will be summarized and discussed in the following paragraphs.

Structure of the siloxane component

^{29}Si NMR, ^{1}H NMR and FTIR experiments reveal the following.

The condensation of the silicon species is almost complete for B1 and decreases slightly when the zirconium content increases. However, the terminal D_1 units represent only a few per cent of the silicon content.

The hydroxyl content of the samples increases with zirconium content. No hydroxyl moiety is detected in B1 by ^{1}H NMR. For B4, there is 5 to 10 wt% water, alcohol or silanol groups remaining in the bulk material. ^{29}Si NMR shows that only a small part of these hydroxyl groups can be assigned to D_1 units. Among the listed hydroxylated species present in the material, the most abundant one is water.

The mean polysiloxane chain length decreases from approximately twenty for B1 to less than three for B4. These estimations do not take into account the possible presence of large PDMS loops. This evolution in chain length from B1 to B4 may be associated with a decrease in the siloxane chain mobility.

Although it is well known that dimethyldiethoxysilane hydrolyzed in acidic conditions forms a small amount of cyclic species, ^{29}Si MAS NMR spectra do not show small cyclic species in the bulk hybrid B1. The zirconium to silicon molar ratio is higher in the final material (even if dried at room temperature) than expected in view of the precursor proportions. The cyclic species containing 3 to 5 silicon atoms are volatile, and could have been lost during the synthesis or the drying of the bulks. Note that there is no silicon loss detected for B1 samples cured at $140\,^{\circ}C$. The small cyclic species have probably been already lost during the drying process.

Redissolution experiments coupled with ^{29}Si NMR allows evaluation of the siloxane chain length for B1. The same order of magnitude of the siloxane length (about 15 Si units instead of about 20) is obtained as from ^{29}Si MAS NMR experiments. Chromatography could probably also be used to shed more light on the siloxane distribution.

Structure of the inorganic domains

FTIR and ^{17}O MAS NMR studies reveal the formation of a zirconium oxo network, whose structure seems unaffected by the siloxane moiety. The structure of the zirconium oxo domains of the B samples is probably as that already described for materials obtained upon hydrolysis of zirconium propoxide. The structure of zirconium oxo polymers and clusters has been extensively reported in the literature.[19,33,41,53,54] Generally in such systems the coordination number of zirconium is mainly 7.[33a,33b,53,54] The Zr–O and Zr–Zr distances range between 2.15–2.30 and 3.4–3.5 Å, respectively, being close to those reported for crystalline zirconium oxides.[53,54]

Density measurements performed on the hybrid bulk samples can be used to estimate the density of the zirconium oxo domains. A calculation has been made by assuming that the densities of each component (siloxane and zirconium oxo domains) are independent of the material composition and that the overall density of the material is the considered mean of the two components densities. Values of 2.5 and 0.9 g cm^{-3} have been found for the zirconium oxide and the siloxane parts respectively. The densities of monoclinic crystallized zirconia and PDMS are 5.3 and 0.95 g cm^{-3}, respectively. Moreover, the density of imperfectly crystallized zirconia nanoparticles has been evaluated to be 2.8 g cm^{-3}.[55] This value is in agreement with the density obtained for the zirconium oxide part in the B hybrid materials. The zirconium oxopolymeric domains are probably formed through cluster assembly. During the aggregation process holes are created, leading to the formation of non-crystalline domains of lower density than zirconia. This assumption is supported by nitrogen absorption–desorption experiments performed on several B samples that show an increase in the measured specific surface with zirconium content. The BET surface is almost zero for B1 and increases up to 30 m^2 g^{-1} for B4 materials.

Interface between siloxane and zirconium oxopolymer domains

In summary, the interactions that take place between the polysiloxane and metal-oxo domains are ionocovalent Si–O–Zr bonds, hydrogen bonds and van der Waals interactions. All three types of interactions coexist in the xerogels, but with variable proportions. The amount of strong interactions (ionocovalent and hydrogen bonds) increases with zirconium content.

β-Diketones such as acetylacetone are known to be good complexing agents of transition metal alkoxides. Upon addition of acetylacetone to a sol containing linked siloxane–zirconium oxo oligomers, the cleavage of Si–O–Zr bonds was revealed by ^{29}Si NMR. In swelled hybrid samples, complexation of zirconium atoms located at the surface of the crosslinking domains made with zirconium oxo species can also occur. This complexation reaction, which leads to the cleavage of Si–O–Zr bonds, seems to be a driving force for the dissolution of the bulk samples. The presence of loops probably favors the swelling of the PDMS regions by the acetylacetone solvent, aiding efficient and fast dissolution.

Size of the domains

SAXS experiments show that B hybrid materials can be classified as nanocomposites with heterogeneity existing on a scale of about 1–2 nanometers. These heterogeneities are zirconium oxo domains separated by a mean distance which decreases from about 5 nm to 1.3 nm as the zirconium content increases.

Good agreement is obtained between SAXS results and straightforward calculations made from a simple model[56] which assumes that zirconium oxo polymers are monodisperse spheres and that they are arranged in a simple cubic packing.

Effect of curing

FTIR, ^{1}H, ^{17}O and ^{29}Si MAS NMR as well as chemical analysis reveal no marked effect of curing at 140 °C on B1. However, an increase of the modulus from 10 MPa up to 60-70 MPa is shown by DMA. Hybrid samples aged or cured at moderate temperatures (room temperature to 140 °C) probably increase their modulus through a slight modification of the interface between siloxane species and zirconium oxo based nanodomains. It can be noted that the 10 MPa modulus value was obtained for a freshly prepared B1 sample, while the modulus of the same sample aged at 60 °C is about 60-70 MPa, as for B1-140 samples. The observed difference of the modulus between B1 and B1-140 can perhaps be assigned to the slow aging of samples dried at room temperature. As the other characterizations were performed on older samples and were reproducible from one sample to another, it can be concluded that the curing at 140 °C leads to only minor changes in B1.

Curing at 200 °C has a greater impact on B1 and B4. Curing aids the loss of silicic species, about 15 wt% for B1 xerogel. This is probably associated with the formation of T and Q crosslinking units as revealed by ^{29}Si MAS NMR. ^{17}O and FTIR results show an increase in the amount of Si–O–Zr bonds for B4-200. Similar behavior was not detected for the B1-200 sample within the limits of the technique sensitivity. This difference of behavior between B1 and B4 upon curing may be explained by changes in the interface with composition. In highly hydrophobic B1 hybrids of low zirconium content, the amount of hydroxyl groups and water molecules at the interface is much lower than for B4. As a result there are not enough nucleophilic species to provide further reactions during post curing. The pronounced increase in modulus of B1-200 xerogel in comparison with B1 is due to an increase of the crosslinking density between siloxane species (T and Q species are thermally formed) rather than an increase in the number of Si–O–Zr bonds.

Conclusions

The polydimethylsiloxane/zirconium oxopolymer materials presented in this work are hybrids which consist of amorphous zirconium oxo domains of about one to two nanometers in diameter. The mean separation between these domains decreases from about 5 nm to 2 nm when the Zr/Si ratio increases. The siloxane species (chains and loops) have an average length that decreases from about 15–20 to 3 silicon atoms with the zirconium content. The interface between siloxane and zirconium oxo domains is constituted mainly by $Zr–O–Si(CH_3)_2$ bonds and hydrogen bonds, their relative proportion being a function of the zirconium content. The curing of these hybrids at 140 °C completes the drying of the hybrid network, without dramatically affecting the characteristics of the organic–inorganic interface. Aged B1 and B1-140 hybrid materials are stable, transparent and easy to shape. Composed of hydrophobic and hydrophilic nanodomains they are excellent host matrices for studying dye matrix interactions.

Acknowledgement

We gratefully acknowledge J. Maquet for her valuable help in runing NMR experiments, C. Cazeneuve for DMA measurements and R. Campostrini from the Dipartimento di Ingegneria dei Materiali (Trento, Italy) for the TGA measurements coupled with a mass spectrometer.

References

1 (*a*) H. Schmidt and B. Seiferling, *Mater. Res. Soc. Symp. Proc.*, 1986, **73**, 739; (*b*) B. M. Novak, *Adv. Mater.*, 1993, **5**, 422; (*c*) C. Sanchez and F. Ribot, *New J. Chem.*, 1994, **18**, 1007; (*d*) U. Schubert, N. Hüsing and A. Lorenz, *Chem. Mater.*, 1995, **7**, 2010; (*e*) D. A. Loy and K. J. Shea, *Chem. Rev.*, 1995, **95**, 1431.
2 S. Kohjiya, K. Ochiai and S. Yamashita, *J. Non-Cryst. Solids*, 1990, **119**, 132.
3 C. L. Schutte, J. R. Fox, R. D. Boyer and D. R. Uhlmann, in *Ultrastructure Processing of Advanced Materials*, ed. D. R. Uhlmann and D. R. Ulrich, J. Wiley & Sons, New York, 1992, p. 95.
4 M. Spinu and J. E. McGrath, *J. Inorg. Organomet. Polym.*, 1992, **2**, 103.
5 S. Motakef, T. Suratwala, R. L. Rocone, J. M. Boulton, G. Toewee and D. R. Uhlmann, *J. Non-Cryst. Solids*, 1994, **178**, 37.
6 J. Hyeon-lee, L. Guo, G. Beaucage, M. A. Macip-Boulis and A. J. M. Yang, *J. Polym. Sci. Part B*: *Polym. Phys.*, 1996, **34**, 3073.
7 J. D. Mackenzie, Q. Huang and T. Iwamoto, *J Sol–Gel Sci. Technol.*, 1996, **7**, 151.
8 N. Yamada, I. Yoshinaga and S. Katayama, *J. Mater. Chem.*, 1997, **7**, 1491.
9 (*a*) G. L. Wilkes, B. Orler and H.-H. Huang, *Polymer Prepr.*, 1985, **26**, 300; (*b*) H.-H. Huang, B. Orler and G. L. Wilkes, *Macromolecules*, 1987, **20**, 1322.
10 (*a*) G. S. Sur and J. E. Mark, *Eur. Polym. J.*, 1985, **21**, 1051; (*b*) J. E. Mark and J. L. Sullivan, *J. Chem. Phys.*, 1977, **66**, 1006; (*c*) A. L. Andrady, M. A. Llorente and J. E. Mark, *J. Chem. Phys.*, 1980, **72**, 2282.
11 (*a*) *Better Ceramics Through Chemistry VI*, ed. A. Cheetham, C. J. Brinker, M. MacCartney and C. Sanchez, *Mater. Res. Soc. Symp. Proc.*, 1994, **346**; (*b*) *Better Ceramics Through Chemistry VII*, ed. B. K. Coltrain, C. Sanchez, D. W. Schaefer and G. L. Wilkes , *Mater. Res. Soc. Symp. Proc.*, 1996, **435**; (*c*) *Hybrid Materials*, ed. R. Laine, C. Sanchez, C. J. Brinker and E. Gianellis, *Mater. Res. Soc. Symp. Proc.*, 1998, **519**.
12 (*a*) *Sol–Gel Optics I*, ed. J. D. Mackenzie and D. R. Ulrich, *Proc. SPIE*, 1990, **1328**; (*b*) *Sol–Gel Optics II*, ed. J. D. Mackenzie, *Proc. SPIE.* 1992, **1758**; (*c*) *Sol–Gel Optics III*, ed. J. D. Mackenzie, *Proc. SPIE*, 1994, **2288**; (*d*) *Sol–Gel Optics IV*, ed. J. D. Mackenzie, E. J. A. Pope, H. K. Schmidt and M. Yamane, *Proc. SPIE*, 1997, **3136**.
13 B. Schaudel, C. Guermeur, C. Sanchez, K. Nakatani and J. Delaire, *J. Mater. Chem.*, 1997, **7**, 61.
14 S. Diré, F. Babonneau, C. Sanchez and J. Livage, *J. Mater. Chem.*, 1992, **2**, 239.
15 F. Babonneau, *Polyhedron*, 1994, **13**, 1123.
16 F. Babonneau, L. Bois, J. Livage and S. Diré, *Mater. Res. Soc. Symp. Proc.*, 1993, **286**, 289.
17 (*a*) F. Babonneau, *New J. Chem.*, 1994, **18**, 1065; (*b*) F. Babonneau, in *Better Ceramics Through Chemistry VI*, ed. A. Cheetham, C. J. Brinker, M. MacCartney and C. Sanchez, *Mater. Res. Soc. Symp. Proc.*, 1994, **346**, 949.
18 B. Alonso, J. Maquet, B. Viana and C. Sanchez, *New J. Chem.*, 1998, **8**, 935.
19 S. Diré, F. Babonneau, G. Carturan and J. Livage, *J. Non-Cryst. Solids*, 1992, **147&148**, 231.
20 C. Gueurmeur, C. Sanchez, B. Schaudel, K. Nakatani, J. A. Delaire, F. Del Monte and D. Levy, in *Sol–Gel Optics IV*, ed. J. D. Mackenzie, E. J. A. Pope, H. K. Schmidt and M. Yamane, *Proc. SPIE*, 1997, **3136**, 10.
21 Q. Hibben, E. Lu, Y. Haruvy and S. E. Weber, *Chem. Mater*, 1994, **6**, 761.
22 B. Lebeau, J. Maquet, C. Sanchez, E. Toussaere, R. Hierle and J. Zyss, *J. Mater. Chem.*, 1994, **4**, 1855.
23 (*a*) W. Noll, in *Chemistry and Technologies of Silicones*, Academic Press, New York, 1968 (*b*) *Silicon Based Polymer Science*: *A Comprehensive Resource*, ed. J. M. Zeigler and F.W. Gordon Fearon, Advanced Chemistry Series 224, ACS, Washington DC, 1990.
24 D. Massiot, H. Thiele and A. Germanus, *Bruker Rep.*, 1994, **140**, 43.
25 J. Lambart and T. Zemb, *J. Phys.*, 1992, **2**, 1191.
26 A. Bertoluzza, C. Fagnano, M. A. Morelli, V. Gottardi and M. Guglielmi, *J. Non-Cryst. Solids*, 1982, **48**, 117.
27 P. G. Harrison, C. C. Perry and D. A. Creaser and X. Li, *Eurogel'91 proceedings*, Elsevier, North-Holland, Amsterdam, 1992, p. 175.
28 (*a*) M. Schraml-Marth, K. L. Walther, A. Wokaun, B. E. Handy

and A. Baiker, *J. Non-Cryst. Solids*, 1992, **143**, 93; (*b*) A. Matsuda, T. Kogure, Y. Matsuno, S. Katayama, T. Tsuno, N. Tohge and T. Minami, *J. Am. Ceram. Soc.*, 1993, **76**, 2899–2903.
29 M. Andrianainarivelo, R. Corriu, D. Leclercq, P. Hubert Mutin and A. Vioux, *J. Mater. Chem.*, 1996, **6**, 1665.
30 I. M. Miranda Savado, C. J. Serna and J. M. Fernandez Navarro, *J. Non Cryst. Solids*, 1988, **100**, 330.
31 Q. Deng, K. A. Mauritz and R. B. Moore, in *Hybrid Organic–Inorganic Composites*, ed. J. E. Mark, C. Y.-C. Lee and P. Bianconi, *ACS Symp. Ser.*, 1994, **585**, 66.
32 R. E. Richards and H. W. Thompson, *J. Am. Chem. Soc.*, 1947, **69**, 124.
33 A. Lee Smith and D. R. Anderson, *Appl. Spectrosc.*, 1984, **38**, 822; (*a*) C. Sanchez and M. In, *J. Non-Cryst Solids*, 1992, **147&148**, 1; (*b*) C. Sanchez, M. In, P. Toledano and P. Griesmar, *Mater. Res. Soc. Symp. Proc.*, 1992, **271**, 669; (*c*) P. Papet, N. Lebars, J. F. Baumard, A. Lecomte and A. Dauger, *J. Mater. Sci.*, 1989, **24**, 3850; (*d*) J. C. Debsikbar, *J. Non-Cryst. Solids*, 1986, **87**, 343.
34 R. K. Harris and M. L. Robbins, *Polymer*, 1978, **19**, 1123.
35 (*a*) E. Lippmaa, M. Mägi, A. Samoson, G. Engelhardt and A. R. Grimmer, *J. Am. Chem. Soc.*, 1980, **102**, 4889; (*b*) G. Engelhardt, H. Jancke, E. Lippmaa and A. Samoson, *J. Organomet. Chem.*, 1981, **210**, 295; (*c*) M. Mägi, E. Lippmaa, A. Samoson, G. Engelhardt and A. R. Grimmer, *J. Phys. Chem.*, 1984, **88**, 1518; (*d*) R. H. Glaser, G. L. Wilkes and C. E. Bronnimann, *J. Non-Cryst. Solids*, 1989, **113**, 73.
36 G. Champetier and L. Monnerie in *Intoduction à la Chime Macromoléculaire*, Masson, Paris, 1969.
37 R. C. Fay and T. J. Pinnavaia, *Inorg. Chem.*, 1968, **7**, 508.
38 M. In, C. Gerardin, J. Lambard and C. Sanchez, *J. Sol–Gel Sci. Technol*., 1995, **5**, 101.
39 L. Delattre and F. Babonneau, *Chem. Mater.*, 1997, **9**, 2385.
40 T. J. Barstow and S. N. Stuart, *Chem. Phys.*, 1990, **143**, 459.
41 T. J. Barstow, M. E. Smith and H. J. Whitfield, *J. Mater. Chem*., 1992, **2**, 989.
42 P. J. Dirken, R. Dupree and M. E. Smith, *J. Mater. Chem*., 1995, **5**, 1261.
43 J. Blanchard, S. Barboux-Doeuff, J. Maquet and C. Sanchez, *New J. Chem*., 1995, **19**, 929.
44 J. Livage, M. Henry and C. Sanchez, *Prog. Solid. State Chem.*, 1988, **18**, 259.
45 F. Babonneau, J. Maquet and J. Livage, *J. Sol–Gel Sci. Technol.*, 1995, **55**, 53.
46 T. A. Ulibarri, G. Beaucage, D. W. Schaefer, B. J. Oliver and R. A. Assink, *Mater. Res. Soc. Symp. Proc.*, 1992, **274**, 85.
47 (*a*) R. H. Glaser and G. L. Wilkes, *Polym. Bull.*, 1988, **19**, 51; (*b*) H. H. Huang, G. L. Wilkes and J. G. Carlson, *Polymer*, 1989, **30**, 2001.
48 W. McCarthy, J. E. Mark and D. W. Schaefer, *J. Polym. Sci. B*, 1998, **36**, 1167.
49 G. Beaucage, T. A. Ulibarri, E. P. Black and D. W. Schaefer, in *Hybrid Organic–Inorganic Composites*, ed. J. E. Mark, C. Y. Lee and P. A. Bianconi, *ACS Symp. Ser.*, 1995, **585**, 97.
50 L. Bois, J. Maquet, F. Babonneau, H. Mutin and D. Bahloul, *Chem. Mater.*, 1994, **6**, 796.
51 S. J. Clarson, in *Siloxane Polymers*, ed. S. J. Clarson and J. A. Semlyen, Prentice Hall, Englewood Cliffs, NJ, 1993, p. 216.
52 F. Surivet, T. M. Lam, J. P. Pascault and C. Mai, *Macromolecules*, 1992, **25**, 5742.
53 G. Kickelbick and U. Schubert, *Chem. Ber./Recueil*, 1997, **130**, 473.
54 P. Toledano, M. In and C. Sanchez, *C.R. Acad. Sci.*, 1990, **311**, 1161.
55 V. Peyre, PhD, University of Paris VI, 1996.
56 S. Wu, *Polymer*, 1985, **26**, 1855.

Paper 8/07310D